Bull. Mater. Sci., Vol. 36, No. 3, June 2013, pp. 353–359. © Indian Academy of Sciences.

Pt–Ru decorated self-assembled TiO_2–carbon hybrid nanostructure for enhanced methanol electrooxidation

K G NISHANTH[1], P SRIDHAR[1,*], S PITCHUMANI[1] and A K SHUKLA[2]

[1]CSIR-Central Electrochemical Research Institute - Madras Unit, CSIR Madras Complex, Chennai 600 113, India
[2]Solid State and Structural Chemistry Unit, Indian Institute of Science, Bangalore 560 012, India

MS received 28 March 2012; revised 1 May 2012

Abstract. **Porous titanium oxide–carbon hybrid nanostructure (TiO_2–C) with a specific surface area of 350 m^2/g and an average pore-radius of 21·8 Å is synthesized via supramolecular self-assembly with an *in situ* crystallization process. Subsequently, TiO_2–C supported Pt–Ru electro-catalyst (Pt–Ru/TiO_2–C) is obtained and investigated as an anode catalyst for direct methanol fuel cells (DMFCs). X-ray diffraction, Raman spectroscopy and transmission electron microscopy (TEM) have been employed to evaluate the crystalline nature and the structural properties of TiO_2–C. TEM images reveal uniform distribution of Pt–Ru nanoparticles (d_{Pt-Ru} = 1·5–3·5 nm) on TiO_2–C. Methanol oxidation and accelerated durability studies on Pt–Ru/TiO_2–C exhibit enhanced catalytic activity and durability compared to carbon-supported Pt–Ru. DMFC employing Pt–Ru/TiO_2–C as an anode catalyst delivers a peak-power density of 91 mW/cm^2 at 65 °C as compared to the peak-power density of 60 mW/cm^2 obtained for the DMFC with carbon-supported Pt–Ru anode catalyst operating under similar conditions.**

Keywords. **DMFC; anode catalyst; methanol oxidation; Pt–Ru; accelerated durability test.**

1. Introduction

Direct methanol fuel cells (DMFCs) are attractive for portable power applications owing to the easy transportation, storage and refuelling of methanol in conjunction with their reduced system, weight, size, high energy-efficiency and low-temperature operation (Scott and Shukla 2006; Nishanth *et al* 2011a). However, to improve the commercial viability of DMFCs, there are several scientific issues, viz. methanol crossover, sluggish electrode kinetics and durability, which need to be addressed with concomitant improvements in performance characteristics (Nishanth *et al* 2011b). One of the main drawbacks of DMFCs is insufficient activities of the anode catalysts towards methanol oxidation reaction (MOR). It is known that platinum is the only single-component catalyst that shows an excellent catalytic activity towards methanol electro-oxidation, especially at lower temperatures. However, pure platinum is susceptible to CO poisoning during the oxidation of methanol at low temperatures, resulting in a substantial decrease in its activity (Wang *et al* 2008). In order to improve the activity and CO-tolerance of the Pt catalysts, efforts on alloying Pt with other transition metals, viz. Ru, Mo, Sn, etc have been expended. In general, CO-poisoned platinum can be regenerated via the reaction of surface CO with oxygen species associated with an element like Ru, Mo, etc to yield CO_2. The addition of a metal to Pt-based catalysts significantly lowers the overpotential for methanol electrooxidation through the bi-functional mechanism. Pt–Ru is recognized as the most promising anode electro-catalyst for DMFCs because of its superior CO tolerance due to a bi-functional effect, where CO is oxidized by OH species generated by water discharge on Ru surface atoms. But the CO tolerance of the Pt–Ru is still unsatisfactory for practical DMFC applications. To this end, it is necessary to further the catalytic activity of Pt–Ru catalyst (He *et al* 2007; Tian *et al* 2007).

It has been reported that the addition of transition metal oxides such as CeO_2, TiO_2, WO_3, MoO_3, etc to Pt–Ru could improve CO tolerance and MOR activity (Park *et al* 2004; Song *et al* 2006; Sun *et al* 2010). Transition metal oxides are demonstrated to be good surface promoters for improving Pt activity towards methanol oxidation due to their special 'spill-over' effect (Hepel *et al* 2007). Among these metal oxides, TiO_2 seems to be a promising candidate owing to its natural abundance, cost, semiconductivity and stability in acidic environments (Shanmugam and Gedanken 2007). The electrode using TiO_2 as the support for platinum changes the electronic property of the Pt surface such that the chemical adsorption of CO on the surface is weakened due to the interaction between TiO_2 and Pt (Shanmugam and Gedanken 2007). It has been reported that there is some co-operative effect for platinum catalyst in the presence of TiO_2 that facilitates oxidation of CO_{ads}. Recent studies have shown an increase in the kinetics of MOR as well as CO tolerance for TiO_2 modified Pt–Ru/C and Pt–Ru/CNT (Hepel *et al* 2007). However, for TiO_2 to act as an efficient cooperative catalyst, it is important that the oxide and metal should be in close

*Author for correspondence (psridhar@csircmc.res.in)

contact while allowing diffusion of the fuel to the Pt–Ru catalyst. There are different synthetic strategies like solution-based processing, involving the intimate mixing of Pt, Ru and TiO_2 precursor solution, impregnation and colloidal methods using Pt–Ru/C and TiO_2 particles and physical mixing of Pt–Ru/C with TiO_2 particles adopted to prepare homogenous composite catalyst. Solution-based methods (colloidal, impregnation and sol–gel) seem desirable to achieve nanoscale mixing of the metal and metal–oxide phases. However, these methods involve pyrolysis and a post-pyrolysis heat treatment that may damage Pt–Ru/C (Saida *et al* 2010; Yooa *et al* 2010).

In the light of the foregoing, it is important to develop an effective synthetic method to achieve homogenous nanocomposite catalyst without any post-pyrolysis heat treatment. Accordingly, titanium oxide–carbon nanocomposite with mesoporous structure is directly synthesized as a catalyst support via supramolecular self-assembly with an *in situ* crystallization process in order to achieve high surface area. Active sites on such a porous structure would be easily accessible to the reactant leading to reduced diffusion resistance/mass-transfer resistance. The microstructure, including surface area, morphology and crystallinity, is characterized by Brunauer–Emmett–Teller (BET) method, transmission electron microscopy (TEM), X-ray diffraction (XRD) and Raman spectroscopy. Pt–Ru on titanium oxide–carbon composite is prepared by chemical impregnation using $NaBH_4$ as a reducing agent. The crystalline nature and alloy formation are confirmed by XRD studies, while the morphology and particle-size distribution are determined by TEM. Methanol electrooxidation and accelerated durability test (ADT) are performed using cyclic voltammetry (CV). The catalysts are performance-tested in DMFCs at 65 °C using methanol as fuel and oxygen as an oxidant.

2. Experimental

2.1 *Synthesis of titanium dioxide–carbon hybrid nanostructure*

Porous titania–carbon hybrid nanostructure was prepared using supramolecular self-assembly method followed by an *in situ* crystallization. In brief, a tri-block copolymer Pluronic F127 was dissolved in ethanol followed by the addition of titanium isopropoxide at room temperature under constant stirring (solution A). Subsequently, phloroglucinol and pluronic F127 were dissolved in a solution containing ethanol and water in 10:9 ratios by weight. Subsequently, HCl was added to the solution as a catalyst. The solution was stirred at room temperature for additional 30 min till a light pink colour appeared. This was followed by adding formaldehyde to the above admixture (solution B). Solution A was dropped into solution B and stirred at room temperature for 2 h. The homogeneous mixture was dried overnight at 40 °C. After drying, the product was heated at 100 °C for 8 h and ground into powder. Calcination was carried out in a tubular furnace under nitrogen atmosphere at a flow rate of 100 mL/min. The heating program started from ambient temperature to 500 °C at 1 °C/min, 500 °C–1000 °C at 2 °C/min and then kept at 1000 °C for 3 h, followed by cooling to room temperature. After heat treatment, the solids were ground, washed with hot distilled water and dried. In the subsequent section, titanium oxide-carbon composite is denoted as TiO_2–C.

2.2 *Preparation of supported Pt–Ru*

30 wt% Pt–Ru (1:1) supported on TiO_2–C or Vulcan XC-72R carbon black was used as a catalyst. Sodium borohydride ($NaBH_4$) was used to reduce H_2PtCl_6 and $RuCl_3$. At first, the support was suspended in deionized water and subjected to ultrasonication for 20 min. Precursors of Pt and Ru were added to the resulting ink and mixed for 15 min. Subsequently, the temperature was raised to 80 °C followed by the addition of $NaBH_4$ solution. After 45 min, the prepared catalysts were filtered and washed with boiling water and dried.

2.3 *Physical characterizations*

X-ray diffraction (XRD) patterns for the catalysts were recorded on the Xpert Highscore Plus instrument using CuKα radiation ($\lambda = 1{\cdot}5406$ Å) between 20° and 90° in reflection geometry in steps of 5° min^{-1}. FT–Raman spectrometer (FRA 106 Brüker) was employed to characterize TiO_2–carbon nanostructure. Nitrogen adsorption–desorption isotherms were measured at 77 K using a Micromeritics ASAP 2020. Total surface area and pore volume were determined using the single-point method and the Brunauer–Emmett–Teller (BET) equation, respectively. Pore-size distribution (PSD) data were obtained by Barrett–Joyner–Halenda (BJH) method and the position of the maximum of the PSD was used as the average pore diameter. The structure and morphology of the hybrid material and electro-catalysts were analysed using transmission electron microscopy (TEM).

2.4 *Electrochemical measurements*

Electrochemical measurements were performed with an electrochemical analyser (Autolab PGSTAT-30), using a conventional three-electrode test cell with a saturated calomel electrode (SCE) and a platinum foil as the reference and counter electrodes, respectively. A glassy-carbon (GC) disk with geometrical area of 0·071 cm^2 was polished using alumina slurry to a mirror finish followed by washing with water and acetone. High-purity nitrogen was used for de-aeration of the solution. All experiments were carried out at 25 ± 2 °C. The working electrodes were prepared as follows. 15 mg of supported catalyst, 1·5 mg

of 5 wt% nafion solution (DuPont, USA) and 3 ml of ultrapure water were mixed ultrasonically; 20 μL suspension was quantitatively transferred to the surface of the freshly-polished glassy-carbon disk. The electrode was dried at room temperature. Prior to any electrochemical measurement, the working electrode was cycled between −0·25 and 0·8 V with respect to SCE at a sweep rate of 50 mV/s. Experiments were conducted in nitrogen-purged blank (0·5 M $HClO_4$) electrolyte for removing any contaminant from the electrode and activating it. Catalytic activities of MOR on the catalysts were performed by CV. To obtain reproducible and reliable results, CV experiments were performed in a fresh solution containing 0·5 M CH_3OH and 0·5 M $HClO_4$ in the potential range between −0·23 and 1 V vs SCE at a scan rate of 50 mV/s for 20 cycles for every measurement. Accelerated durability testing (ADT) on electro-catalysts was carried out in a solution containing 0·5 M $HClO_4$ and 0·5 M CH_3OH in a potential cycle between 0·36 and 0·86 V vs SCE at a scan rate of 10 mV/s for 1000 cycles. The amount of Ru leached out during ADT from the catalysts was estimated by ICP–MS analysis. The actual composition was obtained from the calibration curves of the known standards.

2.5 *Preparation of membrane electrode assembly and testing*

The catalysts were evaluated in DMFCs by making membrane electrode assemblies (MEAs). MEA consisted of a membrane sandwiched between an anode and a cathode. Both the anode and cathode comprised of a backing layer, a gas-diffusion layer (GDL) and a catalyst layer. Teflonized Toray carbon paper of thickness 0·37 mm was used as the backing layer. For the diffusion layers, carbon slurry was prepared by dispersion of Vulcan XC 72R in 2-propanol with poly-tetrafluoroethylene (PTFE) emulsion under ultrasonication. The resultant slurry was applied onto the macroporous support with a loading of 1·5 mg/cm^2 on both the electrodes followed by sintering at 350 °C for 30 min. The loading of Pt and nafion in anode catalyst layer was kept at 1 mg/cm^2 and 10 wt%, respectively while that in the cathode catalyst layer was kept at 2 mg/cm^2 and 30 wt%, respectively. A thin layer of nafion ionomer was applied to the catalyst surface of both the electrodes. MEAs were obtained by hot pressing the nafion-117 membrane (Du Pont, USA) sandwiched between cathode and anode under 15 kN (60 kg/cm^2) at 130 °C for 2 min. The geometrical area of all the MEAs used in the present study was 4 cm^2. MEA performances were evaluated using a conventional fuel cell and fixture with a parallel serpentine flow-field machined on graphite plates. The cells were tested at 65 °C and at atmospheric pressure with 2 M aqueous methanol at a flow rate of 2 sccm at the anode side while the flow rate of oxygen was kept at 200 sccm at the cathode side. The galvanostatic polarization data were recorded using a LCN100-36 electronic load procured from Bitrode Corporation. The reproducibility of the data was ascertained by repeating the experiments at least twice.

3. Results and discussion

XRD patterns for titanium oxide–carbon composite samples (figure 1) reveal well resolved, sharp peaks that are consistent with crystalline–rutile titanium oxide phase. However, a small amount (<20%) of anatase phase is also present in the composite. It has been reported that the anatase phase is found even after heating to 1100 °C in the presence of carbon (Tsumura *et al* 2002; Liu *et al* 2008; Zhang *et al* 2008).

Raman spectroscopy is employed to confirm the crystalline phase of TiO_2 and the existence of carbon in the composite. Figure 2 shows presence and nature of the carbon in the composite. Raman spectra show a characteristic *G*-band at 1591 cm^{-1} and a *D*-band at 1337 cm^{-1}, suggesting that the carbon exhibits both graphitic and non-graphitic forms. The bands at 435 and 607 cm^{-1} exhibit characteristics of rutile TiO_2 (Abazovic *et al* 2009; Cao *et al* 2010).

Nitrogen adsorption–desorption isotherm given in figure 3(a) conforms to type IV isotherm revealing mesoporous nature of the adsorbent. The data on TiO_2–carbon hybrid nanostructure exhibit a well-defined step at approximately 0·40–0·80 P/P^0, which is associated with the filling of mesopores due to capillary condensation. The specific BET surface area for TiO_2–C is 350 m^2/g. It is interesting to note that specific surface area of commercially available Vulcan XC 72R is only 230 m^2/g. Barret–Joyner–Halenda (BJH) pore-size distribution analysis (figure 3(b)) shows the pores of 21·8 Å radii to be dominant.

Figure 4 shows images of TiO_2–C hybrid nanostructures. The planar views of nanostructured TiO_2–C show that the titania nanocrystals are embedded into the carbon framework (figure 4a). The data show that the titanium species are highly dispersed in the polymer and/or carbon framework during the self-assembly of the microstructures. The high resolution TEM reveals the crystalline nature of the nano-structured hybrid material. The lattice fringe can

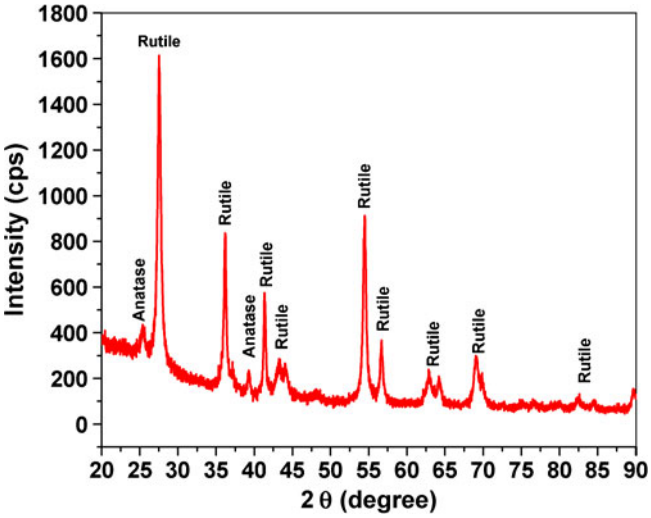

Figure 1. Powder XRD pattern for TiO_2–carbon hybrid nanostructure.

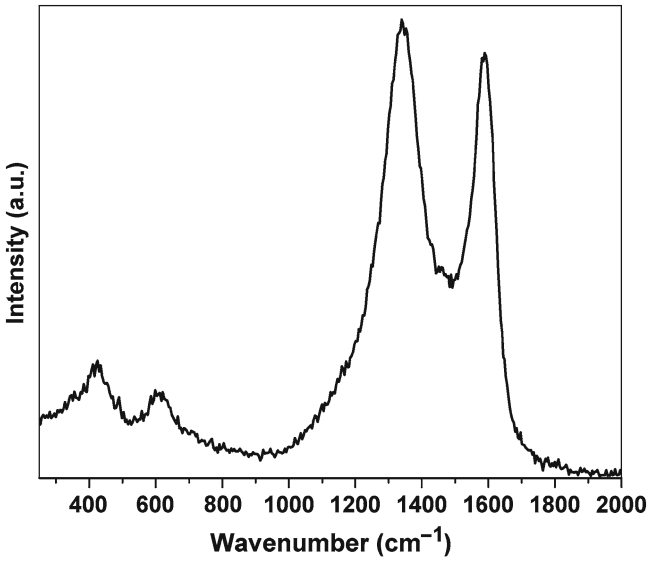

Figure 2. Raman spectra for TiO_2–carbon hybrid nanostructure.

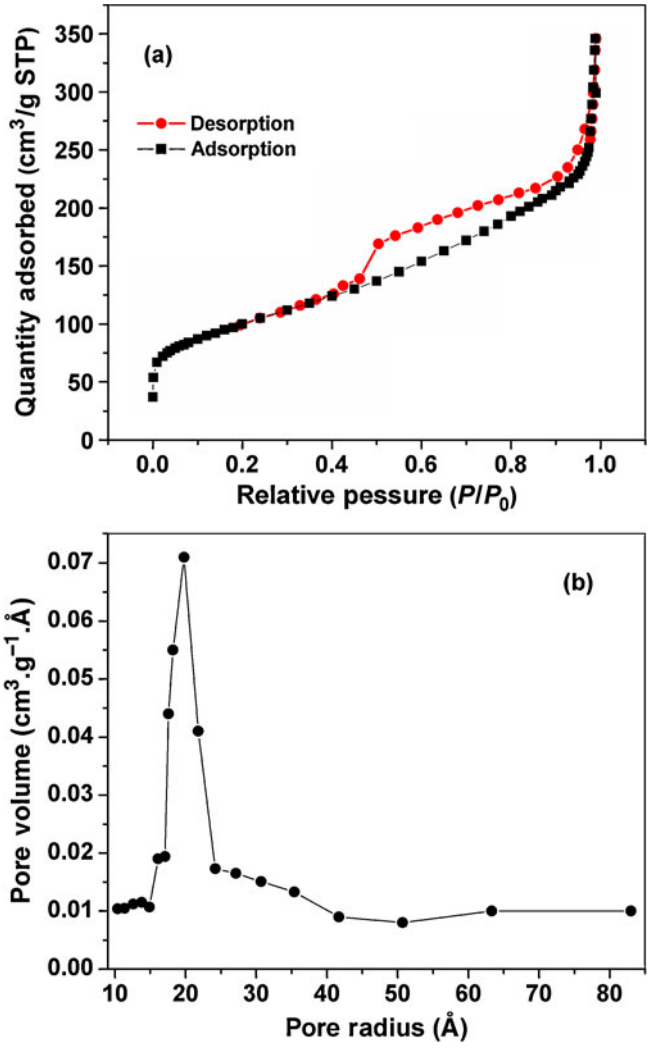

Figure 3. (**a**) Nitrogen sorption isotherm and (**b**) corresponding pore-size distribution data for TiO_2–carbon hybrid nanostructure.

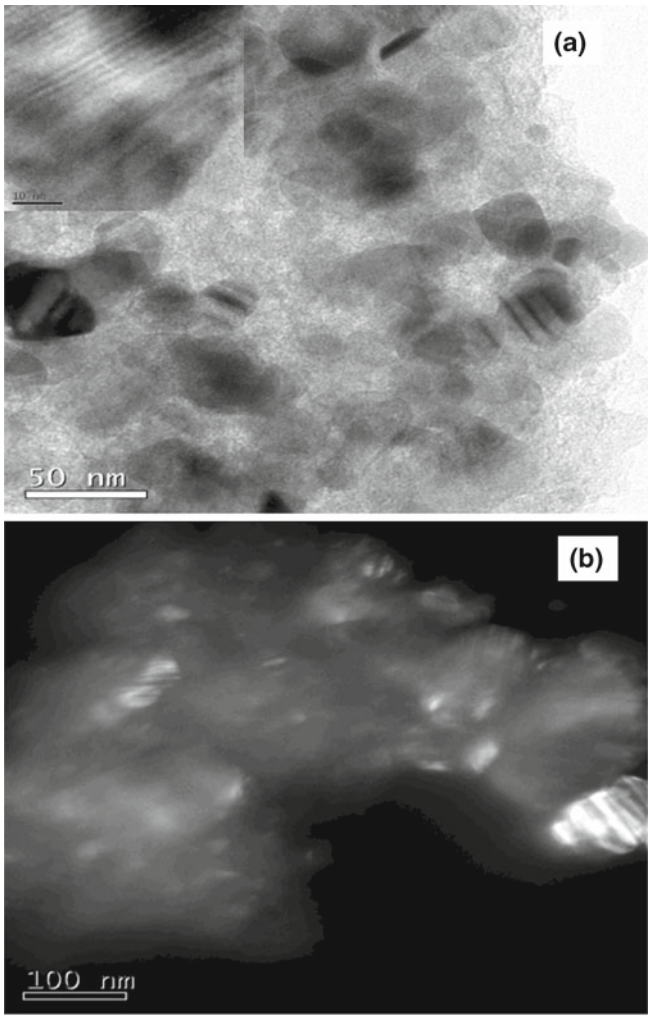

Figure 4. (**a**) TEM image for TiO_2–carbon hybrid nanostructure, inset: corresponding HRTEM and (**b**) dark-field TEM image of TiO_2–carbon hybrid nanostructure.

be clearly measured in TEM images with average d-spacing of 0·332 nm. The dark-field TEM image (figure 4b) further confirms crystalline TiO_2 nanoparticles (bright spot) spreading over the carbon surface.

Figure 5 shows XRD patterns for Pt and Pt–Ru deposited on TiO_2–C composite. XRD patterns of Pt/C and Pt on TiO_2–C catalysts exhibit diffraction peaks of (111), (200) and (220) at 2θ values of 39·75, 46·23 and 67·42°, respectively. These peaks indicate that Pt is present in the face-centred cubic (*fcc*) structure. The diffraction patterns obtained for Pt–Ru/TiO_2–C are similar to those for Pt, except that the corresponding 2θ values are higher. The shift caused by the incorporation of Ru in the *fcc* structure of Pt reveals that a single-phase Pt–Ru is formed on TiO_2–C. TEM study is conducted to ascertain the degree of dispersion, particle-size distribution and average particle size of Pt–Ru electrocatalyst. It is clearly seen from figure 6 that Pt–Ru nanoparticles (d_{Pt-Ru} = 1·5–3·5 nm) are uniformly dispersed on TiO_2–C.

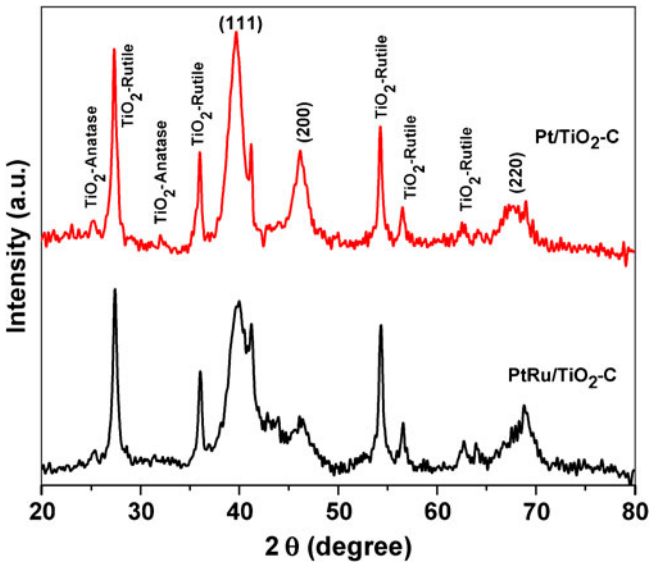

Figure 5. Powder XRD pattern for Pt and Pt–Ru deposited on TiO_2–carbon hybrid nanostructure.

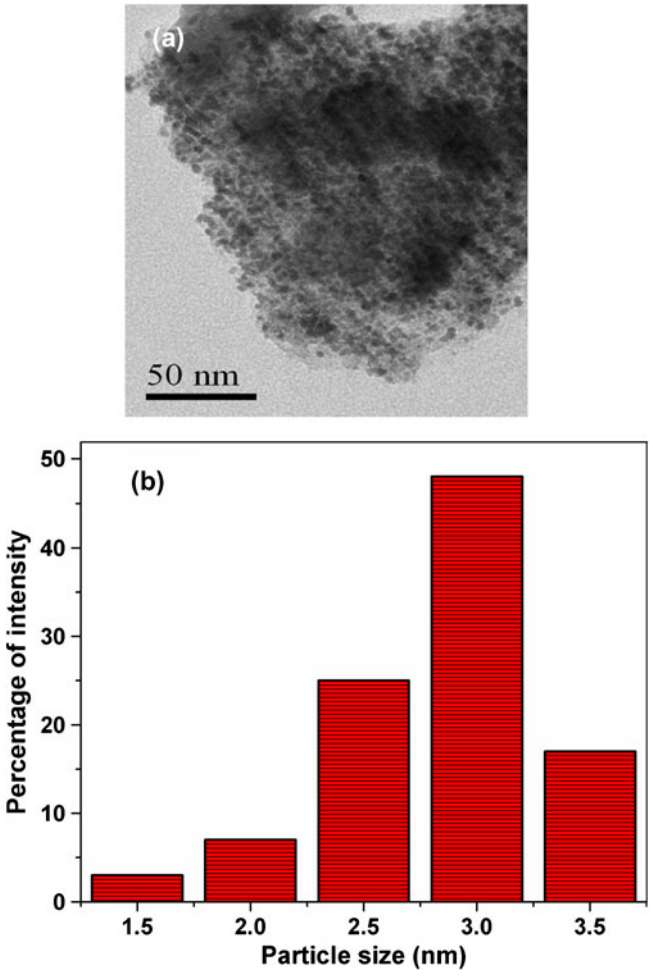

Figure 6. (**a**) TEM image for Pt–Ru on TiO_2–carbon hybrid nanostructure and (**b**) corresponding particle–size distribution of Pt–Ru on TiO_2–carbon hybrid nanostructure.

Electro-catalytic activities for Pt–Ru/C and Pt–Ru/TiO_2–C catalysts for methanol oxidation reaction have been studied by cyclic voltammetry in 0·5 M aq. CH_3OH solution containing 0·5 M $HClO_4$ at a scan rate of 50 mV/s. The resulting voltammograms are shown in figure 7. It is clear that TiO_2–C supported electro-catalyst shows higher catalytic activity in relation to Pt–Ru on carbon. The current density for methanol oxidation reaction on TiO_2–C supported catalyst is higher than the carbon supported electro-catalyst. The peak potentials for methanol adsorbate oxidation for Pt–Ru supported on TiO_2–C and carbon are 0·52 and 0·57 V, respectively; the negative potential shift for TiO_2–C supported catalysts in relation to carbon-supported catalyst indicates that methanol oxidation occurs at a lower potential. To further substantiate the observed data, methanol electrooxidation studies are conducted on carbon and TiO_2–C supported Pt. Figure 8 shows methanol adsorbate electrooxidation peak potential for TiO_2–C supported Pt at 0·83 V and for carbon supported Pt at 0·93 V. Moreover, TiO_2–C supported Pt shows higher current density at lower potential. The negative shift in the methanol adsorbate electrooxidation peak potential and higher current demonstrates the superior electro-catalytic activity for TiO_2–C supported Pt. The higher activity is likely due to enhanced electrochemical surface area as evident from H_{upd} region in figure 7, in addition to the modification of electronic structure of Pt nanoparticles due to interaction with titanium oxide, which leads to a change in the adsorption characteristic of methanol on Pt/TiO_2–C (Shanmugam and Gedanken 2007). Furthermore, the hydroxylated Ti might facilitate the adsorption of methanol accelerating its diffusion. The concentration of methanol at the interface is increased due to enhanced chemisorption on TiO_2–C composite in comparison with that

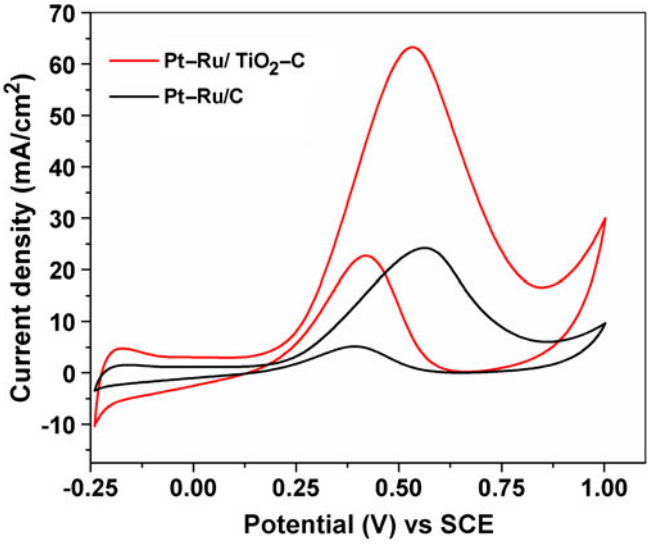

Figure 7. Cyclic voltammograms for methanol electrooxidation on Pt–Ru/C and Pt–Ru/TiO_2–C in N_2-saturated aqueous solution containing 0·5 M $HClO_4$ and 0·5 M CH_3OH at a scan rate of 50 mV/s.

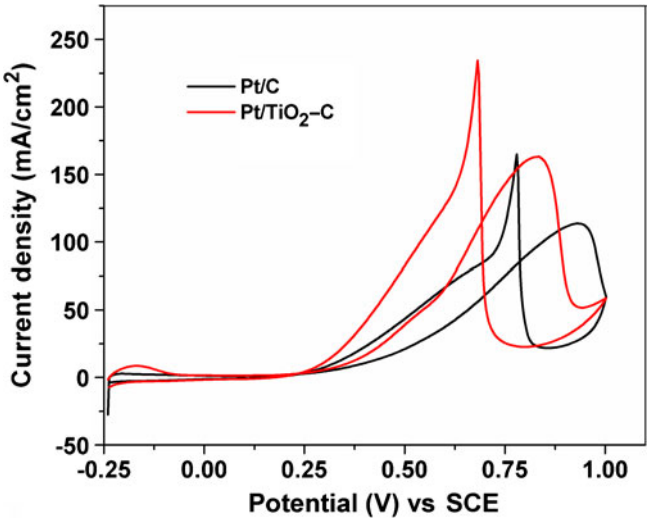

Figure 8. Cyclic voltammograms for methanol electrooxidation on Pt/C and Pt/TiO_2–C.

on Vulcan XC 72. It is reported that active oxygen containing surface species are necessary for the oxidative removal of CO-like poisoning intermediates on Pt surface (Saida *et al* 2010). It is reported that there is some cooperative effect for platinum catalyst in presence of TiO_2, which facilitates oxidation of adsorbed CO. In this catalytic system, TiO_2–C and Ru display anti-poisoning function, the carbon network benefits the electron transfer and Pt works as the main dehydrogenation site (Shanmugam and Gedanken 2007).

The electrochemical stability for Pt–Ru/TiO_2–C is evaluated by an accelerated durability test and compared with Pt–Ru/C. Figure 9 shows CVs for methanol oxidation on Pt–Ru/C and Pt–Ru/TiO_2–C before and after the durability study. It is seen that the methanol adsorbate electrooxidation peak shifts from 0·57 to 0·79 V after ADT for carbon supported catalyst, while, for TiO_2–C supported catalyst, the peak potential shifts from 0·52 to 0·55 V after 1000 cycles. The potential shift for carbon supported catalyst after ADT is 220 mV while for TiO_2–C supported catalyst it is only 30 mV. The extent of increased positive potential shift in the case of carbon supported Pt–Ru, indicates decreased catalytic activity towards methanol electrooxidation after ADT. Furthermore, the positive onset potential shift and higher current at peak potential after ADT suggest increased platinum character caused by a continuous Ru metal loss from Pt–Ru (Jusys *et al* 2002; Nishanth *et al* 2010, 2012). By contrast, TiO_2–C supported electro-catalyst shows only a small shift in onset potential and oxidation potential of methanol adsorbate after ADT. This is corroborated by ICP–MS analysis, which shows the concentration of leached out Ru to be: Pt–Ru/C (46 ppb) > Pt–Ru/TiO_2–C (14 ppb). These data suggest that the activity retention rate for TiO_2–C supported catalysts is superior than carbon supported catalyst. These data confirm the enhanced electrochemical stability of the Pt–Ru/TiO_2–C catalyst towards methanol electrooxidation reaction. The stability may be due to the excellent corrosion

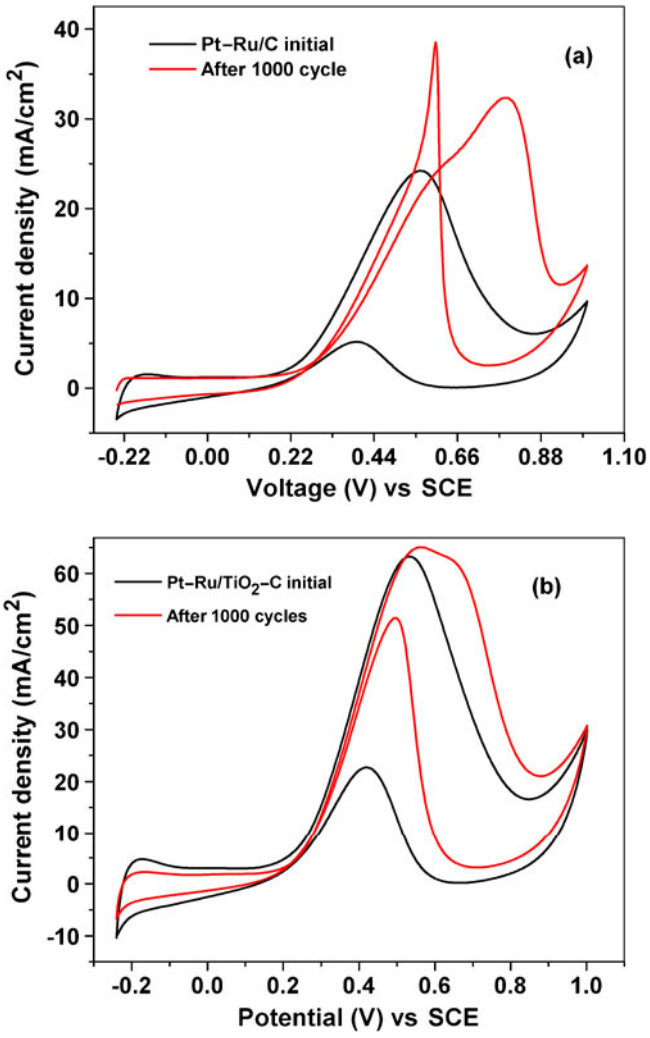

Figure 9. Cyclic voltammograms for methanol electrooxidation on (**a**) Pt–Ru/C and (**b**) Pt–Ru/TiO_2–C catalysts before and after ADT.

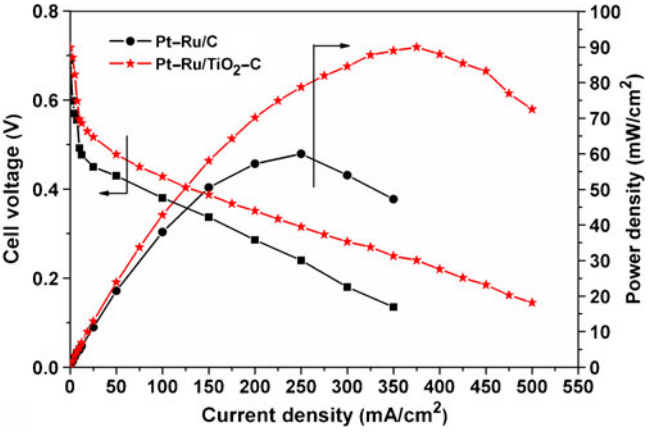

Figure 10. Steady-state performance for DMFCs having Pt–Ru/TiO_2–C and Pt–Ru/C as anode catalysts at 65 °C.

tolerance of titanium oxide–carbon composite in comparison to carbon black in acidic medium. The improved durability for TiO_2–C supported electro-catalysts may be due to the strong interaction between Pt–Ru nanoparticles and TiO_2 support; it would be less likely for Pt–Ru atoms on TiO_2–C to agglomerate to produce larger particles that would cause gradual decrease in electrochemical activity or metal dissolution from the support surface (Cao *et al* 2010).

The catalysts have also been performance tested in DMFCs. The cell polarization data for DMFCs comprising Pt–Ru/TiO_2–C and Pt–Ru/C anode catalysts are given in figure 10. It is clear that the DMFC comprising TiO_2–C supported anode catalyst is superior in performance as compared to DMFC with carbon-supported Pt–Ru. The peak power densities are 91 and 60 mW/cm^2 for DMFCS with Pt–Ru/TiO_2–C and Pt–Ru/C, respectively. These data are in conformity with CV data. Since cathode catalyst and membrane during the study are kept identical, the enhanced performance for the DMFC with TiO_2–C supported catalyst is a clear manifestation of the improved methanol electrooxidation behaviour.

4. Conclusions

In this study, a porous TiO_2–C with a specific surface area of 350 m^2/g is synthesized and investigated as an anode support material for DMFCs. TEM images reveal uniform distribution of Pt−Ru nanoparticles (d_{Pt-Ru} = 1·5–3·5 nm) on TiO_2–C. Methanol oxidation and accelerated durability study for Pt–Ru/TiO_2–C show enhanced catalytic activity and durability in relation to the carbon supported Pt–Ru. DMFC employing Pt–Ru/TiO_2–C as anode catalyst delivers a peak-power density of 91 mW/cm^2 at 65 °C as compared to the peak-power density of 60 mW/cm^2 obtained for the DMFC with carbon supported Pt–Ru catalyst under similar conditions. The improved catalytic activity and durability of TiO_2–C supported electro-catalysts over carbon-supported catalyst suggests that the former is a superior catalyst support for anode electro-catalysts in DMFCs.

Acknowledgements

Financial support from CSIR, New Delhi, through a Supra Institutional Project under EFYP is gratefully acknowledged. (KGN) gratefully acknowledges MNRE, New Delhi, for the award of a Senior Research Fellowship.

References

Abazovic N D, Mirenghi L, Jankovic I A, Bibic N, Sojic D V, Abramovic B F and Comor M I 2009 *Nanoscale Res. Lett.* **4** 518

Cao F F, Wu X L, Xin S, Guo Y G and Wan L J 2010 *J. Phys. Chem.* **C114** 10308

He D, Yang L, Kuang S and Cai Q 2007 *Electrochem. Commun.* **9** 2467

Hepel M, Dela I, Hepel T, Luo J and Zhong C J 2007 *Electrochim. Acta* **52** 5529

Jusys Z, Kaiser J and Behm R J 2002 *Electrochim. Acta* **47** 3693

Liu R, Ren Y, Shi Y, Zhang F, Zhang L, Tu B and Zhao D 2008 *Chem. Mater.* **20** 1140

Nishanth K G, Sridhar P, Pitchumani S and Shukla A K 2010 *ECS Transactions* **33** 2027

Nishanth K G, Sridhar P, Pitchumani S and Shukla A K 2011a *J. Electrochem. Soc.* **158B** 871

Nishanth K G, Sridhar P and Pitchumani S 2011b *Electrochem. Commun.* **13** 1465

Nishanth K G, Sridhar P, Pitchumani S and Shukla A K 2012 *Fuel Cells* **12** 146

Park K W, Choi J H, Ahn K S and Sung Y E 2004 *J. Phys. Chem.* **B108** 5989

Saida T, Ogiwara N, Takasu Y and Sugimoto W 2010 *J. Phys. Chem.* **C114** 13390

Scott K and Shukla A K 2006 *Direct methanol fuel cell fundamentals, problems and perspective in modern aspects of electrochemistry*, (eds) R E White *et al* (New York: Springer) p. 127

Shanmugam S and Gedanken A 2007 *Small* **3** 1189

Song C, Kanfar M and Pickup P G 2006 *J. Appl. Electrochem.* **36** 339

Sun Z, Wang X, Liu Z, Zhang H, Yu P and Mao L 2010 *Langmuir* **26** 12383

Tian J, Sun G, Jiang L, Yan S, Mao Q and Xin Q 2007 *Electrochem. Commun.* **9** 563

Tsumura T, Kojitani N, Izumi I, Iwashita N, Toyodad M and Inagakie M 2002 *J. Mater. Chem.* **12** 1391

Wang Z, Chen G, Xia D and Zhang L 2008 *J. Alloys Compd.* **450** 148

Yooa S J, Jeonb T Y, Choc Y H, Leeb K S and Sung Y E 2010 *Electrochim. Acta* **55** 7939

Zhang L W, Fu H B and Zhu Y F 2008 *Adv. Funct. Mater.* **18** 2180